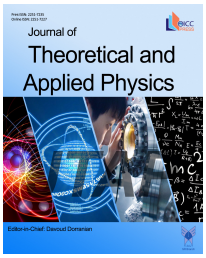

Volume 18, Issue 1, 182407 (1-12)

Journal of Theoretical and Applied Physics (JTAP)

https://dx.doi.org/10.57647/j.jtap.2024.1801.07

Synthesis and characterization of TiO_2-Ag-chitosan nano-composites in order to surface modification and bone tissue engineering using dip coating method

Salahaldin Mansur Alduwaib*, Safaa Abed Salih, Dina Jalal Al-den Fakar Al-den

Department of Sciences, Collage of Basic Education, Al-Mustansiriyh University, Baghdad, Iraq.

***Corresponding author:** salah.aldin@uomustansiriyah.edu.iq

Original Research

Received:
30 July 2023
Revised:
22 September 2023
Accepted:
9 October 2023
Published online:
10 January 2024

Abstract:

In this research, titanium dioxide (TiO_2) nanopowder, TiO_2-Ag (TA) and TiO_2-Ag-CH (TACH) nanocomposite were produced by the hydrothermal method. After the synthesis of nanoparticles and nanocomposites, the skull titanium mesh implant pieces were immersed in solutions containing nanopowders of TiO_2, TA, and TACH and coated using the dip coating method. Structural, chemical, and antibacterial properties of these nanocomposites were characterized using X-ray diffraction (XRD), field emission scanning electron microscope (FESEM), tunneling electron microscopy (TEM), Fourier transform infrared (FTIR) spectroscopy, and Raman analysis. Specific surface area was determined by the Brunauer-Emmett-Teller analysis (BET) method and the antibacterial properties of the coated implants were investigated using the disk diffusion method.Based on the antibacterial results, it has been observed that the TA and TACH nanocomposites have effectively inhibited bacterial growth, as evidenced by the clear non-growth halo around the bacteria in the growth inhibition halo images. TACH nanocomposite showed the highest antibacterial property and TiO_2 nanoparticle had the lowest antibacterial property on both Escherichia coli (*E. coli*) and Staphylococcus aureus (*S. aureus*).

Keywords: Titanium dioxide (TiO_2) nanopowder; Hydrothermal method; Antibacterial properties

1. Introduction

One of the most important issues in discussions about human health is the failure of a part of the body or tissue, which causes many problems for the patient. In order to treat such problems, a part of the patient's body or another person's body is transplanted to the damaged area, and sometimes artificial structures made of non-living materials are used. Although these methods may cure the patient, they are sometimes associated with limitations and complications such as infection at the transplant site and tissue rejection [1]. Today, another therapeutic approach called tissue engineering is being developed. Tissue engineering is using a combination of cells, engineering materials and suitable chemical agents to repair, improve, or replace inefficient or disabled tissues in a living organism [2]. In this approach, usually a porous and biodegradable scaffold is typically created and then the desired tissue cells are cultured on it [3]. By controlling the physiological conditions outside the body, primary tissue forms on the scaffold and after implantation inside the body, the scaffold is destroyed by the formation of new tissue [2].

One of the advantages of tissue engineering is that it reduces the number of surgeries required and helps patients recover faster. One of the main factors influencing tissue engineering is the choice of scaffolds used in tissue engineering. A scaffold is a three-dimensional structure that mechanically supports cells [4]. The scaffold must be biocompatible and have desirable mechanical properties, so that it has the ability to withstand forces and provide a behavior similar to the target tissue against stresses [5]. In addition, it should have a controlled degradation rate, proper porosity dimensions and morphology, and possess acceptable sterilization and

grafting capabilities so that it can be used in tissue engineering [3]. So far, many composites made of biodegradable polymers and bioactive ceramics have been used as biocompatible scaffolds in tissue engineering [6]. Therefore, due to an increase in the number of bone injuries and the development of surgeries with minimal damage has been directed research towards the design and manufacture of nanocomposites consisting of biodegradable polymer (Chitosan) and bioactive ceramic (TiO_2) with antibacterial properties (TiO_2, Ag nanoparticle), as a biocompatible scaffold in bone tissue engineering [7]. Titanium dioxide (TiO_2) is a biocompatible compound that has favorable antibacterial properties in addition to bioactive properties and good corrosion resistance [8–10]. TiO_2 is a biocompatible material with desirable bioactive properties, and for this reason, it has favorable bone growth promotion properties and can be used in the form of a three-dimensional structure as a suitable scaffold for bone formation at the site of bone defects [11], [12]. Other bio-ceramics, such as hydroxyapatite and bioactive glass, have no antibacterial effect despite their excellent bioactivity, while titanium dioxide is a bioactive ceramic with an antibacterial effect in vivo [13]. In addition, the addition of TiO_2 nanoparticles to chitosan-based coatings improves the antibacterial and mechanical properties and thus increases the stability of the coating [14, 15].

Among other biodegradable materials, biocompatible/biodegradable polymers, including chitosan, are usually flexible but do not have sufficient strength compared to bone. In bio/medical applications, chitosan has several applications (such as drug encapsulation and tissue engineering scaffolds) [16, 17]. On the other hand, due to the similarity of chitosan to the extracellular matrix of bone and cartilage, as well as having unique physical and chemical properties such as biocompatibility, non-toxicity, biodegradability, biological function, antibacterial activity and chemical resistance, it is used as a coating material to modify the surface of orthopedic implants [17, 18]. Also, nanocomposites made of bio-ceramics and biodegradable polymers have been widely used to prepare absorbable scaffolds in bone tissue engineering, to provide temporary mechanical support to the damaged tissue, and to provide the conditions for tissue regeneration. In addition, such scaffolds provide the possibility of releasing the desired elements or compounds in the place and eventually being removed. Therefore, there will be no need for secondary surgery [19, 20]. On the other hand, hybrid composites can be made with organic-organic (chitosan-alginate, chitosan-protein and chitosan-starch), organic-inorganic (chitosan-TiO_2, alginate-TiO_2, and starch-TiO_2) and inorganic-inorganic (TiO_2-ZnO, TiO_2-MgO and TiO_2-Ag) compounds and can be prepared using different synthesis methods including intercalation of the polymer, sol-gel, hydrothermal, electrical deposition, chemical and physical vapor deposition, suspension and liquid phase deposition [21–26]. Today, there is a particular interest in combining natural polymers such as chitosan with inorganic materials such as TiO_2 to obtain hybrid composites with useful properties. Also, according to the studies, it was observed that inorganic compounds such as TiO_2 can increase the mechanical, physical and biological properties of this biopolymer (chitosan) [21]. Kumar [7] investigated the use of nano-TiO_2-doped chitosan scaffolds for bone tissue engineering applications. The study found that the interaction between chitosan and nano-TiO_2 made the scaffold highly porous and brittle, which could be an effective substitute for bone tissue engineering. In one of the research projects conducted by Xiao et al. [27], they investigated and made a Chitosan-Ag-TiO_2 three-component hybrid composite against *E. coli*, *S. aureus*, and *C. albicans* bacteria. The results show the synergistic effect of these three components for microbial inactivation and subsequent cell death. Miyazaki et al. [28] emphasized that organic-inorganic composites (Chitosan-TiO_2) showed interesting biomedical applications. It has been found that the integration of TiO_2 in a chitosan biopolymer is a new approach to increase the biological activities of this biopolymer.

The purpose of this research is the fabrication and characterization of a new chitosan/titanium dioxide/silver nanocomposite scaffold. Chitosan, as a natural polymer with excellent biocompatibility properties, is combined with a combination of titanium dioxide and silver nanoparticles to be evaluated as a new scaffold for bone tissue engineering. Titanium dioxide nanoparticles show relatively good antibacterial properties and bioactivity, but they are not biocompatible with bone cells. On the other hand, chitosan improves biocompatibility and promotes bone growth in living tissue and has an antibacterial effect in the body. In addition, the silver nanoparticles that are used also possess strong antibacterial properties. Therefore, it is expected that the scaffold investigated in this research for bone tissue engineering will lead to the promotion of bone growth, improvement of antibacterial behavior and bioactivity.

2. Materials, methods of synthesis and characterization

2.1 Raw materials

The titanium precursor, Titanium tetraisopropoxide (TTIP), was used in the synthesis of the nanocomposites. Chitosan and silver nitrate were also used as precursors and were purchased from Merck Company, Germany. Acetic acid, nitric acid, and ethanol were obtained from the Mojalali brand, Iran.

2.2 Methods of synthesis

2.2.1 Synthesis of TiO_2 solution

In this research, titanium dioxide (TiO_2) nano-powder was produced by the hydrothermal method. In the first step, 5 mL of ethanol was mixed with 5 mL of acetic acid and stirred with a magnetic stirrer for 15 min. Then, 5 mL of titanium tetraisopropoxide was quickly added to it and stirred for another 15 min to complete the reaction between the two materials. In the next step, 100 mL of deionized water was quickly added to it to complete the hydrolysis reaction between the two materials, and then, 2 mL of concentrated nitric acid was added to it. In the next step, the solution was placed in an oil bath under reflux conditions to be heated in a controlled temperature condition. In the reflux procedure, heating is uniformly and indirectly applied to the solution. The solution was placed at 80 °C for one hour. After one

hour, the color of the solution changed from white to pale blue.
A 100 mL autoclave with stainless steel material was used to perform the hydrothermal process. Its inner material is made of Teflon, which does not react with the material inside. The final solution was transferred from the reflux into the autoclave and its lid was completely tightened to create the temperature and pressure necessary for the formation of nanoparticles inside the autoclave. The autoclave was placed in an oven at 200 °C for 10 hours.
The material removed from the autoclave has two phases, solid and liquid. The resulting material was stirred a little to make it uniform and then it was placed in a centrifuge to completely separate its solid deposit. The final deposit was washed three times with ethanol. The spin speed of the centrifuge was set at 10000 rpm for 5 min. In the last step, the material washed with ethanol was dried in an oven at a temperature of 60 °C and then ground with a mortar. The final titanium dioxide nano-powder was used for structural and morphological characterization. 0.5 g of synthesized titanium dioxide nano-powder was mixed with 50 mL of deionized water and stirred for 30 min until it was completely dispersed. In the next step, this solution was used to coat the implant pieces.

2.2.2 Synthesis of TA solution

In a 100 mL beaker, 0.1 g of silver nitrate was added to 10 mL of deionized water at room temperature until it was completely dissolved. In the second beaker, 0.5 g of TiO_2 nano-powder was mixed with 50 mL of deionized water and stirred for 30 minutes until it was completely dispersed. The Ag solution was added little by little to the TiO_2 solution under stirring and placed at 70 °C for 15 min until it became completely uniform.

2.2.3 Synthesis of TACH solution

0.5 g of chitosan powder was mixed with 50 mL of deionized water and 0.5 mL of acetic acid at a temperature of 80 °C for 30 minutes until it was completely dissolved. In another beaker, 0.5 g of titanium dioxide nano-powder was mixed with 50 mL of deionized water and stirred for 30 minutes until it was completely dispersed. In third beaker, 0.1 g of silver nitrate was added to 10 mL deionized water and stirred at room temperature. The three solutions were mixed together and placed at 70 °C for 15 min until it became completely uniform.

2.2.4 Coating the implant pieces

skull titanium mesh implant pieces were coated by the dip coating method. The Iranian Toos Nano device was used to carry out the dip coating process. The implant pieces were immersed in the three solutions prepared in the previous steps (TiO_2, TA, TACH). The speed of entering and leaving of the implants into the solution was set at 10 mm/min. Each time, the pieces were placed in the solutions for 10 seconds, and 5 min were considered to dry the solution on the surfaces of the implants. This dip coating process was repeated 50 times. After finishing the coating process, the samples were dried in the oven at 120 °C for 24 hours.

2.3 Characterization method

The X-Ray Diffraction method, D8 Advance Bruker YT model, was used to investigate the structure of the synthesized samples, using CuKα radiation at $\lambda = 1.541$ $\AA$. Field emission scanning electron microscope (FESEM), MIRA3 TESCAN-XMU model, was employed to study the surface morphology of the coated implants. The chemical composition was investigated by Energy-dispersive X-ray spectroscopy (EDX) in the voltage range of $0-10$ kV. Transmission electron microscopy (TEM), EM 208S model, was used to analyze the size and shape of the nano-structures. The chemical bonds of the nano-structures were analyzed by Fourier Transform Infra-Red spectrometer (FTIR), Nicolet AVATAR 370 equipment model. Specific surface area was determined by the Brunauer-Emmett-Teller analysis (BET) method from the N_2 isotherms collected with a Belsorp mini II BEL device, Japan, on degassed samples. In Raman spectroscopy, a laser light beam is applied on the sample and a detector records the wavelength and intensity of the beam emitted from the sample. By measuring the difference in the wavelength of the input and output beam, the type of bonds in the sample can be determined. Raman analysis of the samples was performed by the TakRam N1-541 device, Iran, at a wavelength of 532 nm.
The antibacterial properties of the coated implants have been investigated by disk diffusion and viable cell count. The disk diffusion method is a simple, low-cost, and widely used technique for evaluating the antibacterial properties of materials. In this method, a standard suspension of the desired microorganism is spread on an agar culture medium, and samples containing the antibacterial agent are placed on the culture medium. The antibacterial agent diffuses from the sample into the agar and inhibits the growth of the microorganism. After incubation, the diameter of the zone of inhibition (the area where no bacterial growth occurs) is measured. This method provides a qualitative assessment of the antibacterial activity of the material. Standard gram-negative bacteria *E. coli* ATTC25922 and gram-positive *S. aureus* ATTC25923 were purchased from the Iran Scientific-Industrial Research Center. The concentration of bacteria used was 10^4 CFU/mL. Müller-Hinton Broth culture medium (Merck) was used.

3. Structural characterization

3.1 XRD analysis

X-ray diffraction, which is an old method, is used to study the crystalline properties of nanomaterials. Structural studies of nanocomposites were carried out by examining X-ray diffraction (XRD) spectrum. The X-ray diffraction spectrum was taken in the range of 2θ=10°-90° and with a step of 0.01.
The X-ray diffraction (XRD) patterns of TiO_2, TA, and TACH nanocomposites are shown in Figure 1. All the diffraction peaks of TiO_2 nano-powder show the crystalline structure and the peaks correspond to crystalline planes with angles 2θ=25° (101), 2θ=37.44° (004), 2θ=47.56° (200), 2θ=54.56° (105), 2θ=55.6° (211), 2θ=62.5° (204), 2θ=68.6° (116), 2θ=69.8° (220), 2θ=74.75° (215). All the diffraction peaks define the anatase phase well and can

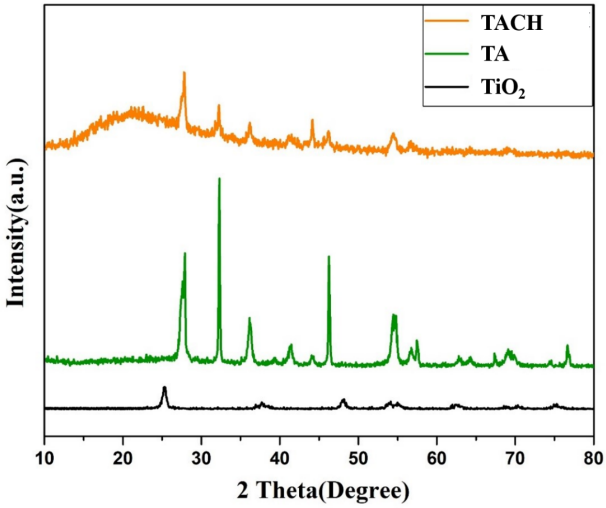

Figure 1. XRD patterns of TiO_2, TA and TACH nanocomposites.

be attributed to the card JCPDS-21-1272 [29]. No distinct peaks related to other crystalline forms were detected in the XRD pattern, indicating the pure nature of the anatase phase of TiO_2 nano-powders.

The X-ray diffraction (XRD) pattern for TA nanocomposite is shown in Figure 1. The XRD pattern of this nanocomposite shows the diffraction peaks that are related to the an anatase-rutile mixed phase. Diffraction peaks observed at 25.4°, 32.5°, 36.3°, 39.1°, 48.5°, 54.8°, 55.5° correspond to the planes 101, 103, 004, 112, 200, 105, and 211, respectively [30, 31]. The diffraction peak at $2\theta = 25.4$ corresponding to plane 101 specifies the crystalline phase of anatase in the nanocomposite [29]. On the other hand, the diffraction peaks at $2\theta = 27.8$, 36.6, 39.3, 41.7, and 57.1 correspond to the 110, 101, 200, 111, and 220 planes of TiO_2 rutile, respectively [29, 31]. In addition, the presence of Ag peaks at 38.2° and 44.3° could not be confirmed by XRD, which could indicate that Ag is highly dispersed in the nanocomposite or there is a possibility that an Ag peak overlaps with the peak of anatase at 38.3°.

The X-ray diffraction (XRD) of the TACH nanocomposite shown in Figure 1 indicates the diffraction peaks of the anatase phase of TiO_2, Ag and CH nanoparticles. These specified peaks corresponded with the previously described peaks of silver nanoparticles reported by Li et al. [32], while the TiO_2 and CH peaks are consistent with the findings of Zafar et al. [33]. It can be seen that the diffraction peaks of this nano-carrier are shifted to a high-angle region, indicating that foreign materials, such as chitosan, introduce stress on the lattice of the host material (Ag/TiO_2). It was also noted that the prominent Ag peak at 38.18° overlapped with the peak of TiO_2 at 38° and suppressed the TiO_2 signal.

3.2 FESEM and EDX analysis

There are various methods to determine the shape and size of grains of the material, one of the most prominent of which is microscopic methods. The Scanning Electron Microscope (FESEM) is one of the most prominent microscopic methods that, in addition to providing the magnified images, can also be used for chemical analysis if equipped with additional equipment. The results of surface morphology of TiO_2, TA and TACH nanocomposites by FESEM are shown in Figure 2. As seen in Figure 2, TiO_2 nanoparticles formed clusters of spherical crystals with a diameter of approximately $0.1 - 0.3$ micrometers and an average particle size of 100 nm. Figure 2 shows the morphology of TA composites. Silver nanoparticles in sizes of 60 to 100 nm are homogeneously distributed in the anatase TiO_2 matrix.

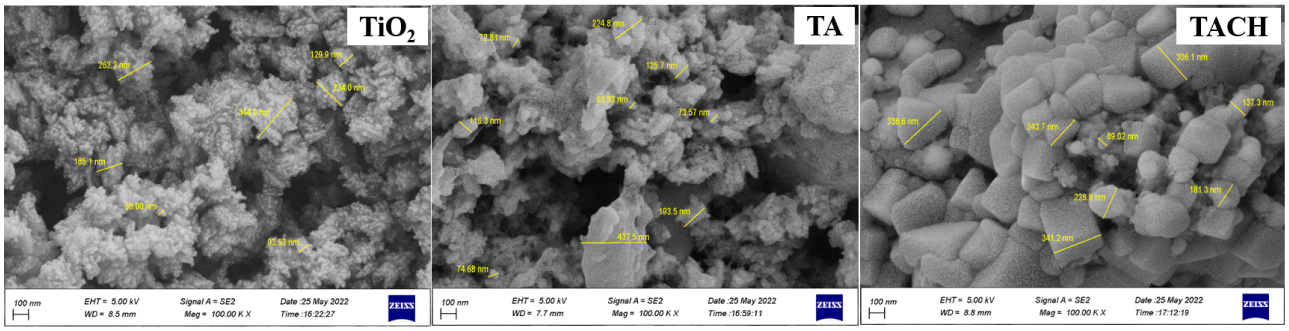

Figure 2. FESEM images of TiO_2, TA and TACH nanocomposites.

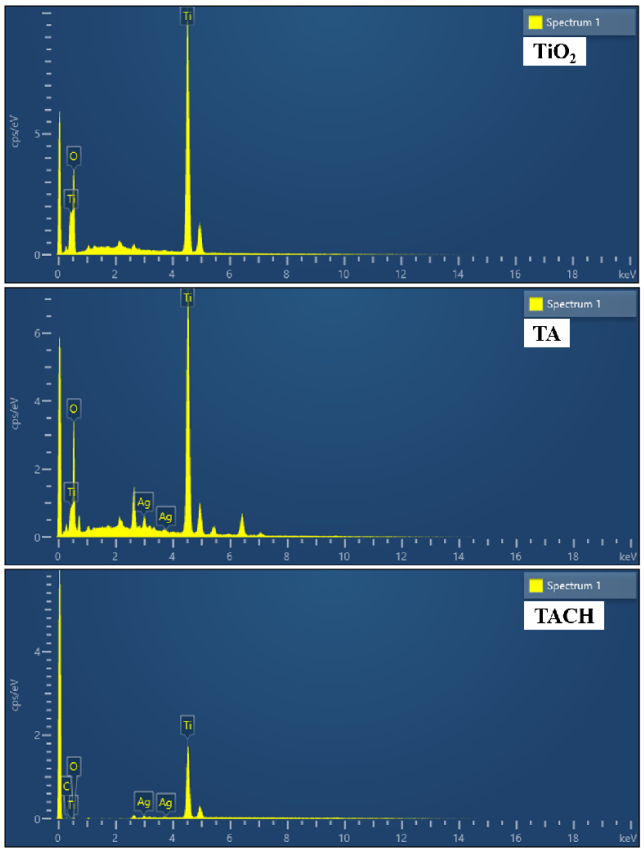

Figure 3. EDX images of TiO_2, TA and TACH nanocomposites.

The EDX spectrum related to this composite is presented in Figure 2. It is clear that the Ag element dominates in the EDX spectrum and confirms the presence of silver nanoparticles in TA nanocomposites. In addition, both Ti and O can be detected in the EDX spectrum.

The morphology of TACH composites is shown in Figure 2. As seen in the Figure, chitosan biopolymer covers the entire surface of TA polygonal nanocomposites. As is evident in the morphology of this composite, silver nanoparticles remain separate on the surface of TiO_2. The elemental spectrum of the synthesized TACH composite is also shown in Figure 2, which shows the peaks related to titanium, silver and chitosan.

EDX analysis was performed to investigate the composition of the grown nanoparticles. Figure 3 shows typical EDX analysis of TiO_2 nanoparticles. From EDX analysis, it is confirmed that the grown nanoparticles are only composed of titanium and oxygen. The Ti:O molar (molecular) ratio of the grown nanoparticles, calculated from EDX and quantitative analysis data, is close to that of bulk. Except for Ti and O, no other peaks were found for any other element in the spectrum, indicating that the grown TiO_2 nanoparticles are pure.

Figure 3 shows the EDX analysis for TA nanocomposites. As can be seen from the figure, the elemental composition of the nanocomposite was confirmed by EDX studies. The presence of TiO_2 elements in the TA nanocomposite is evident in the EDX diagram.

Figure 3 shows the EDX analysis for TACH nanocomposite. As can be seen in the figure, silver and carbon peaks confirm the formation of this nanocomposite structure. In contrast, the peaks of Ti and O elements indicate the characteristic composition of TiO_2.

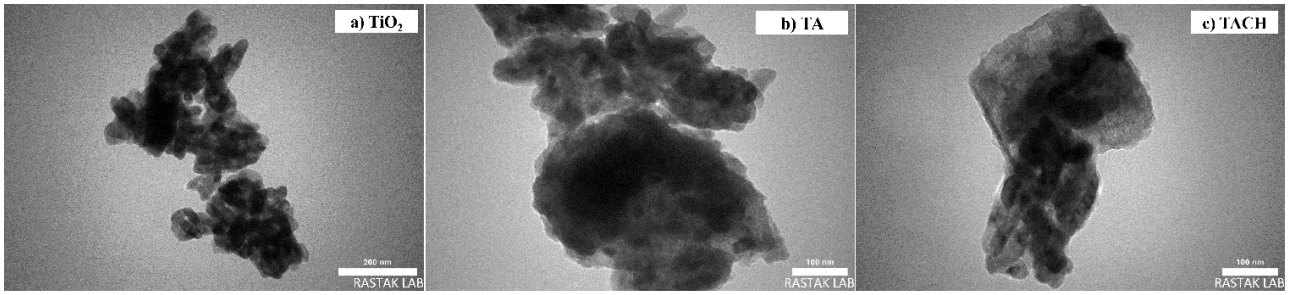

Figure 4. TEM images of TiO_2, TA and TACH nanocomposites.

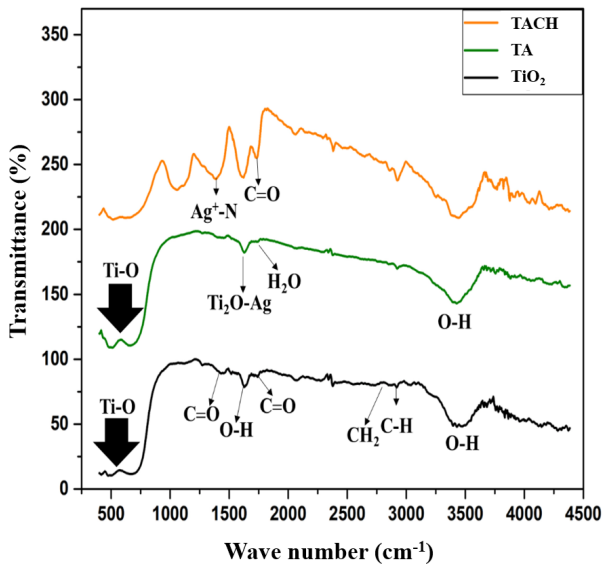

Figure 5. FTIR spectrum of TiO_2, TA and TACH nanocomposites.

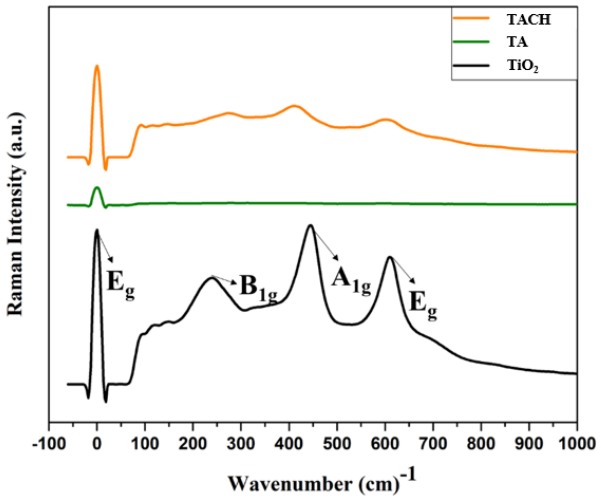

Figure 6. Raman spectrum of TiO_2, TA and TACH nanocomposites.

3.3 TEM analysis

TEM images were taken from the samples, in order to investigate the morphology of the synthesized nanocomposites. TEM images of TiO_2, TA and TACH nanocomposites are shown in Figure 4. The image of TiO_2 nanoparticles can be seen in Figure 4, where the titanium dioxide nanoparticles are spherical in shape and less than 100 nm in size, which have formed inter-connected clusters with a diameter of 0.1 to 0.3 micrometers. Figure 4 shows the image of TA nanocomposite, in which spherical silver nanoparticles with dimensions below 100 nm are homogeneously distributed on TiO_2 nanoparticles. By adding chitosan polymer, it can be seen that according to Figure 4, this polymer covers the entire surface of TA nanocomposites.

3.4 Fourier Transform Infrared spectroscopy analysis (FTIR)

FTIR is a chemical technique used to identify functional groups. This technique can plot the intensity of the infrared spectrum based on the absorption wavelength. In this process, infrared rays from 100 to 10000 cm^{-1} are irradiated to the sample. Some of these rays are absorbed and others pass through the sample. The absorbed rays are converted into rotational and vibrational energy by the sample molecules. Finally, the final signals are displayed by the detector in the range of 400 to 4000 cm^{-1}. It should be noted that each molecule shows its own spectra. Therefore, according to the fingerprint spectra that are specific to each molecule, identification becomes very easy with the help of this analysis. The FTIR spectrum of TiO_2, TA and TACH nanocomposites is shown in Figure 5. As can be seen, FTIR spectroscopy was used to observe the interactions between silver and chitosan nanocomposites and TiO_2 nanoparticles.

Figure 5 shows the FTIR spectrum of TiO_2 nanoparticles. The peaks related to TiO_2 nanoparticles can be seen in the Figure. From this FTIR spectrum, several peaks are visible at 3391.72, 2920.55, 2849.32, 1747.95, 1627.28, 1342.47, 728.77 and 463.88 cm^{-1}. TiO_2 nanoparticles have significant hydroxyl groups on the surface. In addition, small crystals can lead to broad peaks. The spectroscopic band is observed at $\sim$ 3391.72 cm^{-1}, which is related to the symmetric and asymmetric tensile vibrations of the hydroxyl group (Ti-OH) [34].

The broad peak observed between $3600 - 3000$ cm^{-1} is related to the tensile mode of the hydroxyl group O-H, which indicates the presence of moisture in the sample. The characteristic peak at 1627.28 is related to O-H bending vibrations of absorbed water molecules. Therefore, the two peaks observed at 3391.72 and 1627.28 cm^{-1} are related to interfacial (surface) absorbed water and hydroxyl groups [35] and the presence of OH bands in the spectrum was due to chemical and physical absorption of H_2O on the surface of nanoparticles [36]. It has been reported that bands from 400 to 1000 cm^{-1} are attributed to Ti-O tensile and Ti-O-Ti

Table 1. Results obtained from the BET test.

Samples	Average diameter of porosity (nm)	Effective pore volume (cm^3/g)	Effective surface area (m^2/g)
TiO_2	2020.7	0.0072335	0.014319
TA	181.5	0.0075158	0.16564
TACH	106.48	0.0044144	0.16582

bridging modes [37]. For pure TiO_2, the peaks in the range of 400 to 800 cm^{-1} are due to anatase titanium.
Figure 5 shows the FTIR spectrum of TA nanocomposite. The broad peak located at $\sim$ 3439 cm^{-1} is related to the tensile vibration of the hydroxyl group (-OH), which absorbs water and CO_2 molecules in air. And at 1618 cm^{-1}, it originates from the bending vibrations of water molecules [38]. The peak at 1384 cm^{-1} indicates the bonding of the TA composite, confirming that Ag molecules are successfully deposited on TiO_2 particles [39, 40]. The peaks in the range of $500 - 1000$ cm^{-1} are related to the anatase TiO_2 phase [41].
The FTIR spectrum of the TACH nanocomposite is presented in Figure 5. When the physiochemical environment in the vicinity of a functional group changes (for example, complexation between a ligand and a metal ion), accordingly, its characteristic peak changes in position and/or intensity. According to other research [42], chitosan has shown two main peaks at 1642 (C=O tensile) and 1518 cm^{-1} (N-H bending), respectively. In the FTIR spectrum of the nanocomposite, these two peaks were changed to 1692 cm^{-1} and 1516 cm^{-1}, respectively, indicating that silver has bonded with amide on chitosan. In addition, a new high-intensity peak at 1314 cm^{-1} was observed in the nanocomposite, which is possibly attributed to the newly formed Ag^{+}-N coordination bonds [43]. Due to its numerous amine and hydroxyl groups, chitosan has a great affinity for metal ions [44].
Figure 6 shows structural information from Raman spectroscopy for TiO_2, TA and TACH nanocomposites. In Figure 6, four characteristic Raman active modes of anatase TiO_2 with symmetries of E_g, B_{1g}, A_{1g} and E_g were observed at 134, 382, 500 and 618 cm^{-1}, respectively. These vibrational frequencies and their intensity ratios confirm the pure phase of anatase TiO_2 [45].
Raman spectroscopy for TA nanocomposite is also shown in Figure 6 in order to evaluate and identify the phase of nanocomposites. The bands around 153.35, 198.74, 396.32, 521.19 and 637.41 cm^{-1} are characteristic of the anatase TiO_2 phase. However, no signal related to Ag nanoparticles was detected, perhaps due to the relatively low concentration of Ag on TiO_2 and poor dispersion (scattering) of its Raman. The Raman spectrum of the TACH nanocomposite is shown in Figure 6. The bands observed at 147, 398, 516, and 629 cm^{-1} indicate the anatase phase of TiO_2. In fact, these bands can be assigned to the active modes of the O-Ti-O Raman spectrum in the low frequency of the E_g mode and the high frequency of the B_{1g}, A_{1g}, E_g mode. The presence of these peaks confirms the crystallization of the anatase phase of TiO_2.

3.5 Specific surface area measurement (BET)

The BET theory aims to explain the physical absorption of gas molecules on a solid surface and serves as an important analytical technique for measuring the specific surface area of materials. By using BET analysis, it is possible to calculate the percentage of porosity and specific surface area of nanoparticles. BET analysis works based on measuring the volume of nitrogen gas absorbed and desorbed by the surface of the material at a constant temperature of liquid nitrogen.
BET analysis of TiO_2, TA and TACH nanocomposites was performed, as shown in Figure 7. Table 1 shows the properties of TiO_2, TA and TACH nanocomposites, including the effective area, effective porosity volume and the average diameter of porosity using the BET method. According to Table 1, it can be seen that all three nanocomposites have pores larger than 50 nm, so they are in the macro-pore dimensions. The diameter of the pores was significantly decreased by adding silver nanoparticles, and in the presence of chitosan, the diameter of the pores was decreased again. In the presence of silver nanoparticles, the effective area has also significantly increased, and it also shows a slight increase with the addition of chitosan. Based on the shape and position of the pores relative to each other inside the porous material, the pores are divided into the following four categories: passing pores, dead end pores, closed pores, and inter-connected pores. By examining the FESEM images in Figure 2, it turns out that in all three structures, the pores are of the closed type.
In all types of absorption isotherms, as the vapor partial pressure of the absorbate material increases, the amount of absorbed material increases until a monolayer is formed on the surface. Increasing the pressure after this point causes more than one layer to form on the surface. According to the classification by BDDT, the absorption and desorption

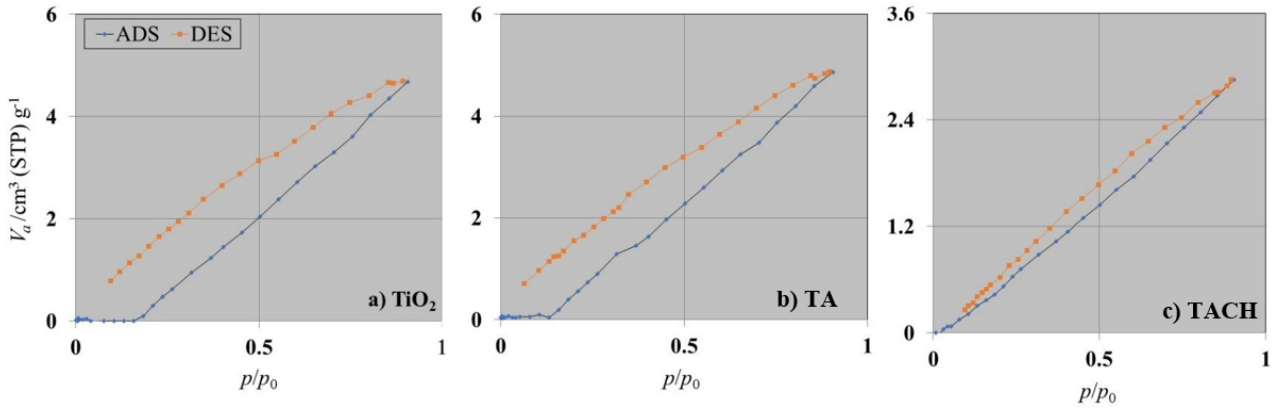

Figure 7. Nitrogen absorption-desorption isotherm for TiO_2, TiO_2-Ag and TACH nanocomposites.

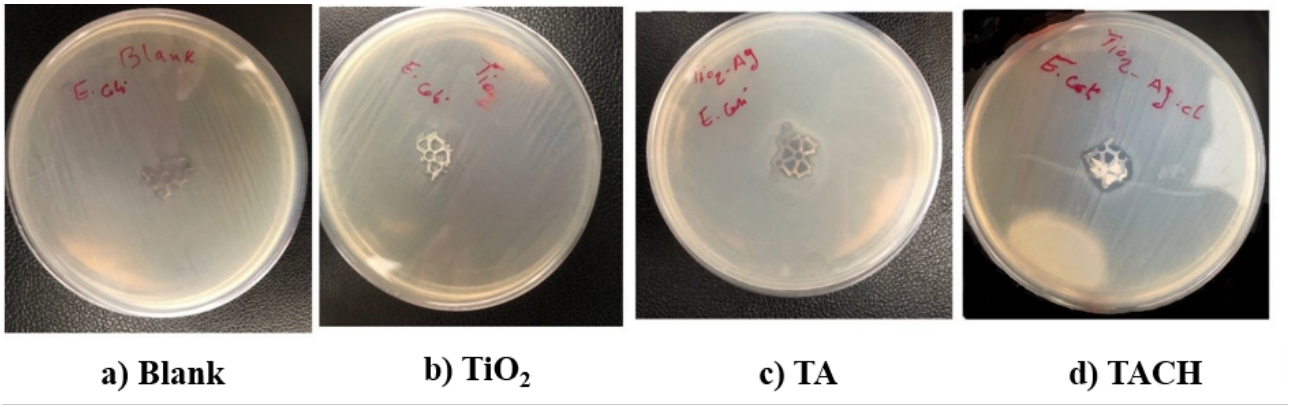

Figure 8. Growth inhibition halo created by disks containing TiO_2, TA and TACH samples on *E. coli*.

isotherm diagrams of TiO_2, TiO_2-CH and TiO_2-PVA follow type 1 and 2, which is specific to non-porous and microporous solid materials [46].

The absorption and desorption diagrams of N_2 of all three nanocomposites showed that in low relative pressure (P/P_0) conditions, the absorption and desorption diagrams do not overlap. This unusual case can occur in materials such as chitosan. Therefore, the excretion process can occur through the penetration mechanism, which encloses the exit of the gas phase from the pores. Confined gases are collected in the pores and simultaneously released under low pressure. Therefore, the absorption-desorption diagram showed that more gases were desorbed than absorbed [47].

3.6 Analysis of the antibacterial property of the samples

The antibacterial test of TiO_2, TA and TACH nanocomposites was performed in the first step by the disk diffusion method. In this method, a standard suspension of the desired microorganism is spread in the Mueller-Hinton agar culture medium, and the samples are then placed on the culture medium and antibacterial agents are spread on it by a sampler. Usually, the antibacterial agent is spread in the agar and prevents the germination and growth of the microorganism, and finally the diameter of the non-growth halo is measured. This method is very popular due to its simplicity, low cost and easy interpretation of the results. In this method, bacteria are classified as sensitive, semi-sensitive or resistant to each antibacterial agent.

Here, the effect of TiO_2, TA, and TACH nanocomposites in solid culture medium was investigated by the disk diffusion method, which included measuring the growth inhibition halo created by disks containing sample on *E. coli* and *S. aureus* bacteria.

The minimum diameter of the inhibited halo was measured after 24 hours and the results are shown in Figures 8 and 9. According to these figure, it is specified that TA and TACH nanocomposites have prevented the bacterial growth and a non-growth halo around bacteria is clearly visible in these images. It can also be seen that the TACH nanocomposite showed the highest antibacterial property and TiO_2 nanoparticles showed the lowest antibacterial property on both *E. coli* and *S. aureus*. In addition, the effect of nanocomposites on *S. aureus* is greater than *E. coli* and it has a larger non-growth halo.

Given that disk diffusion analysis is a qualitative analysis, the viable cell count method was also used to more precisely investigate the antibacterial property of TiO_2, TA and TACH samples. The results are reported in Table 2. According to Table 2, it can be seen that all three samples have antibacterial property against both gram-positive and gram-negative bacteria compared to the blank sample. Similar to the results of disk diffusion, the TACH nanocomposite showed the highest percentage of bacterial growth inhibition and the TiO_2 nanoparticle showed the lowest percentage of bac-

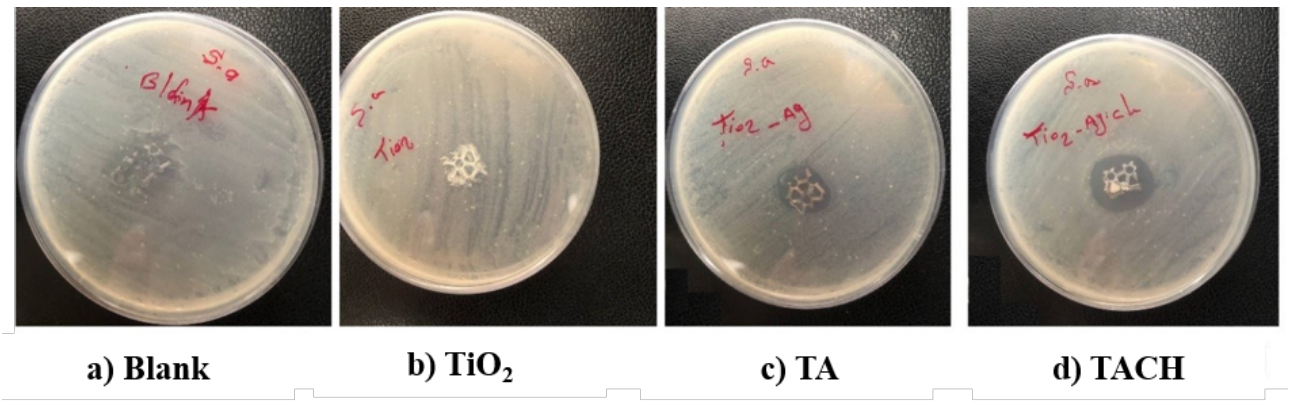

Figure 9. Growth inhibition halo created by disks containing TiO_2, TA and TACH samples on *S. aureus*.

Table 2. Growth inhibition percentage of *E. coli* and *S. aureus* in the presence of TiO_2, TA and TACH samples measured by viable cell count method after 18 hours.

Samples	E. coli	*S. aureus*
Blank	0.0	0.0
TiO_2	48.5	50.8
TA	53.0	63.7
TACH	56.9	71.7

terial growth inhibition on both *E. coli* and *S. aureus*. In addition, the percentage of bacterial growth inhibition by nanocomposites on *S. aureus* is higher than E. coli.
The reports of researchers show that silver nanoparticles and metal oxides such as TiO_2 kill bacteria in different ways. Among them, the penetration of nanoparticles into the bacterial cell and their effect on the cellular DNA causes the death of the bacteria. On the other hand, nanoparticles affect the exchange across the bacterial cell membrane, disturb the activity of cytoplasmic enzymes, and produce the lethal free radicals inside the cell, which causes the destruction of bacteria. The increase in antibacterial property of the TACH nanocomposite is due to the presence of nanoparticles that are uniformly dispersed in the polymer matrix. In fact, the presence of chitosan makes it possible for nanoparticles to have better distribution and dispersion in the polymer matrix. Also, chitosan polymer has effectively reacted via hydrogen bond with nanoparticle plates, which has finally been able to create an inter-connected and uniform structure with the help of transverse connections between polymer strands, which agrees with the results of TEM and FESEM microscopes [48–50].

4. Conclusion

Titanium dioxide (TiO_2) nanopowder, TA and TACH nanocomposites were produced by the hydrothermal method. After the synthesis of nanocomposites, implant pieces were coated by the dip coating method. The skull titanium mesh implant pieces were dipped in solutions containing nanopowders of TiO_2, TA, and TACH to achieve a consistent coating. The X-ray diffraction (XRD) results of TiO_2 show that all the diffraction peaks of TiO_2 nano-powder show a crystalline structure. Also, The XRD pattern of TA nanocomposite shows the diffraction peaks that are related to an anatase-rutile mixed phase. The XRD of TACH nanocomposite indicates the diffraction peaks of anatase phase of TiO_2, Ag and CH nanoparticles. The surface morphology of TiO_2, TA and TACH nanocomposites was characterized using FESEM. The TEM images of TiO_2, TA and TACH nanocomposites show that they are spherical in shape and the size of nanoparticles less than 100 nm. The FTIR spectrum of TiO_2, TA and TACH nanocomposites was used to observe the interactions between silver and chitosan nanocomposites and TiO_2 nanoparticles. The Raman spectroscopy for TiO_2, TA and TACH nanocomposites shows four characteristic Raman active modes of anatase TiO_2 with symmetries of E_g, B_{1g}, A_{1g} and E_g were observed at 134, 382, 500 and 618 cm^{-1}, respectively. BET analysis of TiO_2, TA and TACH nanocomposites included effective area, effective porosity volume and the average diameter of porosity using the BET method. According to the antibacterial results, it is specified that TA and TACH nanocomposites have prevented the bacterial growth and a non-growth halo around bacteria is clearly visible in the images. It can also be seen that TACH nanocomposite showed the highest antibacterial property and TiO_2 nanoparticle the lowest antibacterial property on both *E. coli* and *S. aureus*.

Ethical approval
This manuscript does not report on or involve the use of any animal or human data or tissue. So the ethical approval is not applicable.

Authors Contributions
This report was carried out by the equal contribution of authors.

Availability of data and materials
Research data regarding this manuscript can be shared upon request from corresponding author.

Conflict of Interests
The authors declare that they have no known competing financial interests or personal relationships that could have appeared to influence the work reported in this paper.

References

[1] S. G. Kwon, Y. W. Kwon, T. W. Lee, G. T. Park, and J. H. Kim. "Recent advances in stem cell therapeutics and tissue engineering strategies". *Biomaterials Research*, **22**:1–8, 2018.

[2] S. Caddeo, M. Boffito, and S. Sartori. "Tissue engineering approaches in the design of healthy and pathological in vitro tissue models". *Frontiers in Bioengineering and Biotechnology*, **5**:40, 2017.

[3] J. N Fu, X. Wang, M. Yang, Y. R. Chen, J. Y. Zhang, R. H. Deng, Z. N. Zhang, J. K. Yu, and F. Z. Yuan. "Scaffold-based tissue engineering strategies for osteochondral repair". *Frontiers in Bioengineering and Biotechnology*, **9**:812383, 2022.

[4] A. Eltom, G. Zhong, and A. Muhammad. "Scaffold techniques and designs in tissue engineering functions and purposes: a review". *Advances in Materials Science and Engineering*, **2019**, 2019.

[5] X. Zhao, D. A. Hu, D. Wu, F. He, H. Wang, L. Huang, D. Shi, Q. Liu, N. Ni, M. Pakvasa, Y. Zhang, et al. "Applications of biocompatible scaffold materials in stem cell-based cartilage tissue engineering". *Frontiers in Bioengineering and Biotechnology*, **9**:603444, 2021.

[6] Z. Han H. Qu, H. Fu and Y. Sun. "Biomaterials for bone tissue engineering scaffolds: A review". *RSC Advances*, **9**:26252–26262, 2019.

[7] P. Kumar. "Nano-TiO_2 doped chitosan scaffold for the bone tissue engineering applications". *International Journal of Biomaterials*, **2019**, 2019.

[8] C. L. de Dicastillo, M. G. Correa, F. B. Martínez, C. Streitt, and M. J. Galotto. "Antimicrobial effect of titanium dioxide nanoparticles ". *Antimicrobial Resistance-A One Health Perspective*, , 2020.

[9] L. Yin, Z. Fu, Y. Li, B. Liu, Z. Lin, J. Lu, X. Chen, X. Han, Y. Deng, W. Hu, D. Zou, and C. Zhong. "Enhanced antibacterial properties of biocompatible titanium via electrochemically deposited Ag/TiO_2 nanotubes and chitosan–gelatin–Ag–ZnO complex coating". *RSC Advances*, **9**:4521–4529, 2019.

[10] M. Farrokhi-Rad L. Sorkhi and T. Shahrabi. "Electrophoretic deposition of hydroxyapatite–chitosan–titania on stainless steel 316 L". *Surfaces*, **2**:458–467, 2019.

[11] T. K. Ahn, D. H. Lee, T. Kim, G. Jang, S. J. Choi, J. B. Oh, G. Ye, and S. Lee. "Modification of titanium implant and titanium dioxide for bone tissue engineering". *Novel Biomaterials for Regenerative Medicine*, **1077**:355–368, 2018.

[12] M. Vercellino, G. Ceccarelli, F. Cristofaro, M. Balli, F. Bertoglio, G. Bruni, L. Benedetti M. A. Avanzini, et al. "Nanostructured TiO_2 surfaces promote human bone marrow mesenchymal stem cells differentiation to osteoblasts". *Nanomaterials*, **6**:124, 2016.

[13] Y. Gao, T. Li, S. Duan, L. Lyu, Y. Li, L. Xu, and Y. Wang. "Impact of titanium dioxide nanoparticles on intestinal community in 2, 4, 6-trinitrobenzenesulfonic acid (TNBS)-induced acute colitis mice and the intervention effect of vitamin E". *Nanoscale*, **13**: 1842–1862, 2021.

[14] Z. Dong, R. Li, and Y. Gong. "Antibacterial and freshness-preserving mechanisms of chitosan-nano-TiO_2-nano-Ag composite materials". *Coatings*, **11**: 914, 2021.

[15] Y. Xing, X. Li, X. Guo, W. Li, J. Chen, Q. Liu, Q. Xu, Q. Wang, H. Yang, et al. "Effects of different TiO_2 nanoparticles concentrations on the physical and antibacterial activities of chitosan-based coating film". *Nanomaterials*, **10**:1365, 2020.

[16] R. Parhi. "Drug delivery applications of chitin and chitosan: a review". *Environmental Chemistry Letters*, **18**:577–594, 2020.

[17] L. du Preez J. Fourie, F. Taute and D. De Beer. "Chitosan composite biomaterials for bone tissue engineering—a review". *Regenerative Engineering and Translational Medicine*, :1–21, 2020.

[18] S. Bohara and J. Suthakorn. "Surface coating of orthopedic implant to enhance the osseointegration and reduction of bacterial colonization: A review". *Biomaterials Research*, **26**:26, 2022.

[19] V. J. Cruz-Delgado, N. Rodríguez-Fuentes, V. C. Pat-Cetina, and J. M. Cervantes-Uc. *"Nanocomposites based on biodegradable polymers for biomedical applications"*, volume . Springer, 2023.

[20] J. Tripathy. "Polymer nanocomposites for biomedical and biotechnology applications". *Properties and applications of polymer nanocomposites: Clay and carbon based polymer nanocomposites*, :57–76, 2017.

[21] L. M. Anaya-Esparza, J. M. Ruvalcaba-Gómez, C. I. Maytorena-Verdugo, N. González-Silva, Romero-Toledo, Aguilera-Aguirre, et al. "Chitosan-TiO_2: A versatile hybrid composite". *Materials*, **13**:811, 2020.

[22] I. Nawaz, H. Shehzad, E. Ahmed, A. Sharif, Z. Farooqi, M. Imran Din, R. Begum, A. Irfan, et al. "Facile synthesis and adsorption characteristics of a hybrid composite based on ethyl acetoacetate modified chitosan/calcium alginate/TiO_2 for efficient recovery of Ni (II) from aqueous solution". *Zeitschrift für Physikalische Chemie*, **236**:595–618, 2022.

[23] F. Aydin, E. Yilmaz, G. Demirkiran, Z. Erbaş, M. Vurucuel, and M. Soylak. "TiO_2ZnO nanocomposite: bifunctional material for solid phase extraction of U (VI) and Th (IV) and photocatalytic degradation of organic contaminant". *Journal of Radioanalytical and Nuclear Chemistry*, :1–14, 2023.

[24] W. Al Zoubi, A. A. Salih Al-Hamdani, B. Sunghun, and Y. G. Ko. "A review on TiO_2-based composites for superior photocatalytic activity". *Reviews in Inorganic Chemistry*, **41**:213–222, 2021.

[25] L. M. Anaya-Esparza, Z. Villagran de La Mora, N. Rodríguez-Barajas, T. Sandoval-Contreras, K. Nuño, D. A. López de la Mora, A. Pérez Larios, and E. Montalvo-González. "Protein–TiO_2: A functional hybrid composite with diversified applications". *Coatings*, **10**:1194, 2020.

[26] A. Ujcic, S. Krejcikova, M. Nevoralova, A. Zhigunov, J. Dybal, Z. Krulis, P. Fulin, O. Nyc, and M. Slouf. "Thermoplastic starch composites with titanium dioxide and vancomycin antibiotic: Preparation, morphology, thermomechanical properties, and antimicrobial susceptibility testing". *Frontiers in Materials*, **7**:9, 2020.

[27] G. Xiao, X. Zhang, W. Zhang, S. Zhang, H. Su, and T. Tan. "Visible-light-mediated synergistic photocatalytic antimicrobial effects and mechanism of Ag-nanoparticles@chitosan–TiO_2 organic–inorganic composites for water disinfection ". *Applied Catalysis B: Environmental*, **170**:255–262, 2015.

[28] T. Miyazaki, K. Ishikawa, Y. Shirosaki, and C. Ohtsuki. "Organic–inorganic composites designed for biomedical applications". *Biological and Pharmaceutical Bulletin*, **36**:1670–1675, 2013.

[29] K. Wang, Y. Zhuo, J. Chen, D. Gao, Y. Ren, C. Wang, and Z. Qi. "Crystalline phase regulation of anatase–rutile TiO_2 for the enhancement of photocatalytic activity". *RSC Advances*, **10**:43592–43598, 2020.

[30] M. M. Gui, W. M. P. Wong, S.-P. Chai, and A. R. Mohamed. "One-pot synthesis of Ag-MWCNT@ TiO_2 core–shell nanocomposites for photocatalytic reduction of CO_2 with water under visible light irradiation". *Chemical Engineering Journal*, **278**:272–278, 2015.

[31] C. Zhao, A. Krall, H. Zhao, Q. Zhang, and Y. Li. "Ultrasonic spray pyrolysis synthesis of Ag/TiO_2 nanocomposite photocatalysts for simultaneous H_2 production and CO_2 reduction". *International Journal of Hydrogen Energy*, **37**:9967–9976, 2012.

[32] R. Georgekutty, M. K. Seery, and S. C. Pillai. "A highly efficient Ag-ZnO photocatalyst: synthesis, properties, and mechanism". *Journal of Physical Chemistry C*, **112**:13563–13570, 2008.

[33] N. Zafar, B. Uzair, M. Bilal Khan Niazi, S. Sajjad, G. Samin, M. J. Arshed, and S. Rafiq. "Fabrication & characterization of chitosan coated biologically synthesized TiO_2 nanoparticles against PDR E. coli of veterinary origin". *Advances in Polymer Technology*, **2020**:1–13, 2020.

[34] J. Wei, L. Zhao, S. Peng, J. Shi, Z. Liu, and W. Wen. "Wettability of urea-doped TiO_2 nanoparticles and their high electrorheological effects". *Journal of Sol-Gel Science and Technology*, **47**:311–315, 2008.

[35] A. Kathiravan and R. Renganathan. "Photosensitization of colloidal TiO_2 nanoparticles with phycocyanin pigment". *Journal of Colloid and Interface Science*, **335**:196–202, 2009.

[36] K. Olurode, G. M. Neelgund, A. Oki, and Z. Luo. "A facile hydrothermal approach for construction of carbon coating on TiO_2 nanoparticles". *Spectrochimica Acta Part A: Molecular and Biomolecular Spectroscopy*, **89**:333–336, 2012.

[37] H. Lu, Y. Zhou, S. Vongehr, S. Tang, and X. Meng. "Effects of hydrothermal temperature on formation and decoloration characteristics of anatase TiO_2 nanoparticles". *Science China Technological Sciences*, **55**: 894–902, 2012.

[38] H. Guo, W. Wang, L. Liu, Y. He, C. Li, and Y. Wang. "Shape-controlled synthesis of Ag@ TiO_2 cage-bell hybrid structure with enhanced photocatalytic activity and superior lithium storage". *Green Chemistry*, **15**: 2810–2816, 2013.

[39] E. H. Alsharaeh, T. Bora, A. Soliman, F. Ahmed, G. Bharath, M. G. Ghoniem, K. M. Abu-Salah, et al. "Sol-gel-assisted microwave-derived synthesis of anatase Ag/TiO_2/GO nanohybrids toward efficient visible light phenol degradati". *Catalysts*, **7**:133, 2017.

[40] M. Ganapathy, N. Senthilkumar, M. Vimalan, R. Jeysekaran, and I. V. Potheher. "Studies on optical and electrical properties of green synthesized TiO_2@ Ag core-shell nanocomposite material". *Materials Research Express*, **5**:045020, 2018.

[41] P. R. Griffiths and J. A. de Haseth. *"Fourier Transform Infrared Spectrometry"*, volume **340**. John Wiley & Sons, 1986.

[42] Y. Luo, B. Zhang, W.-H. Cheng, and Q. Wang. "Preparation, characterization and evaluation of selenite-loaded chitosan/TPP nanoparticles with or without zein coating". *Carbohydrate Polymers*, **82**:942–951, 2010.

[43] B. Zhang, Y. Luo, and Q. Wang. "Development of silver/α-lactalbumin nanocomposites: a new approach to reduce silver toxicity". *International Journal of Antimicrobial Agents*, **38**:502–509, 2011.

[44] D. Wei, W. Sun, W. Qian, Y. Ye, and X. Ma. "The synthesis of chitosan-based silver nanoparticles and their antibacterial activity". *Carbohydrate Research*, **344**:2375–2382, 2009.

[45] W. Su, J. Zhang, Z. Feng, T. Chen, P. Ying, and C. Li. "Surface phases of TiO_2 nanoparticles studied by UV Raman spectroscopy and FT-IR spectroscopy". *Journal of Physical Chemistry C*, **112**:7710–7716, 2008.

[46] F. Okusulik and F. B. Emre. "Characterization and photocatalytic properties of TiO2/chitosan nanocomposites synthesized by hydrothermal process". *Turkish Journal of Chemistry*, **40**:28–37, 2016.

[47] B. Thomas and L. K. Alexander. "Enhanced synergetic effect of Cr (VI) ion removal and anionic dye degradation with superparamagnetic cobalt ferrite meso–macroporous nanospheres". *Applied Nanoscience*, **8**:125–135, 2018.

[48] S. H. S. Dananjaya, G. I. Godahewa, R. Jayasooriya, J. Lee, and M. De Zoysa. "Antimicrobial effects of chitosan silver nano composites (CAgNCs) on fish pathogenic Aliivibrio (Vibrio) salmonicida". *Aquaculture*, **450**:422–430, 2016.

[49] A. Arora and G. W. Padua. "Nanocomposites in food packaging". *Journal of Food Science*, **75**:R43–R49, 2010.

[50] M. Maizura, A. Fazilah, M. H. Norziah, and A. A. Karim. "Antibacterial activity and mechanical properties of partially hydrolyzed sago starch–alginate edible film containing lemongrass oil". *Journal of Food Science*, **72**:C324–C330, 2007.